IMAGE, POLAR, and Geosynchronous Observations of Substorm and Ring Current Ion Injection

Submitted to AGU Monograph on the Storm-Substorm Relationship

G. D. Reeves, M. G. Henderson, R. M. Skoug, M. F. Thomsen, J. E. Borovsky, H. O. Funsten

Los Alamos National Laboratory, Los Alamos, New Mexico

P. C:son Brandt, D. J. Mitchell

Johns Hopkins APL, Laurel Maryland

J.-M. Jahn, C. J. Pollock, D. J. McComas

Southwest Research Institute, San Antonio, Texas

S. B. Mende

University of California, Berkeley California

The geomagnetic storm of October 4-6, 2000 provides an exceptionally good opportunity to examine the role of substorms during the storm because of the relatively moderate solar wind driving and because of the excellent set of satellite observations. We show that the entire day of October 4 was characterized a sequence of substorms and a gradual build-up of the storm-time ring current. We examined one of those substorms in some detail showing that it had the expected signatures of a magnetospheric substorm. ENA observations and in situ measurements show that the substorms clearly do provide a mechanism for transporting energetic ions from the magnetotail to the inner magnetosphere. Substorm injections do not, however, provide the only mechanism. As other studies have suggested, the evidence from this storm shows that the presence of a quasi-steady convection electric field plays an additional important role. This is seen through the comparison of Dst which decreases slowly and smoothly over nearly 10 hours with geosynchronous particle injections which occur impulsively at roughly 2-hour intervals producing a "sawtooth" injection profile. Further evidence comes from ENA observations that show both impulsive injection during substorms and continued intensification and eastward expansion in response to convection electric fields. We also investigate the transport and symmetry of the ring current particles. We find that, even more than 10-hours into the storm when Dst had decreased below -100 nT and at least five clear substorm injections had occurred, the ring current remained highly asymmetric with essentially no ENA emissions from the dawn-to-noon sector. We also find that Dst, SYM-H, and ASY-H all respond approximately equally in spite of the fact that there is apparently no symmetric component to the ring current until later in the storm.

1. INTRODUCTION

A central question in the storm-substorm relationship is whether the storm-time ring current is built up solely

through a series of substorm injections, whether other processes are necessary, or even whether substorms themselves are necessary. It is now possible to investigate these questions using a powerful combination of ground-based observations, satellite measurements of the in situ ion populations, global auroral imagers, and global energetic neutral atom images.

The newest component in this "toolbox" are the Energetic Neutral Atom (ENA) images. ENAs are produced when a cold exospheric neutral atom gives up its electron to a trapped energetic ion producing a free energetic neutral atom which can be collected remotely and processed to reveal the global, time-dependent distribution of ions in the inner magnetosphere. Thus, we can supplement the more traditional means of investigating the storm-substorm relationship with ENA images which show the timing and location of substorm injections and their relationship to the build-up and trapping of the ring current. (Throughout this paper we use the term "ring current" to describe the magnetospheric current carriers regardless of whether a closed ring of current has been formed)

Despite it's relatively recent introduction, ENA imaging has already been applied quite successfully to the study of storms and substorms. The first application of ENA observations to geomagnetic storms was reported by Roelof [1987] who used ISEE-1 energetic particle observations to produce ENA images of the storm-time ring current. Later, ENA fluxes from the inner magnetosphere were shown to correspond closely to the ground magnetic perturbations represented by the Dst index [e.g. Roelof et al., 1985; Jorgensen et al., 1997, 2001; C:son Brandt et al., this volume]. Henderson et al. [1997] used the Imaging Proton Spectrometer (IPS) on POLAR to show the first time-dependent images of the substorm injection and further investigated substorm injections using inversion techniques to determine the magnetospheric ion distributions [Henderson et al., 1999, 2000]. Jorgensen et al. [2000] showed statistically that substorm typically produce "bursts" of ENA emissions. The first instrument specifically designed to measure ENAs was flown on the low-altitude Swedish microsatellite, ASTRID [e.g. Barabash et al., 1997, C:son Brandt et al., 2001 a, b] and the recently-launched IMAGE satellite now provides ENA images from a suite of detectors [e.g. Burch et al., 2001] which are providing unprecedented spatial and temporal resolution of the injection and transport of inner magnetospheric ions during storms and substorms [e.g. C:son Brandt et al., 2002].

Two recent studies have used ENA observations and supporting data to look explicitly at the storm-substorm relationship. Reeves and Henderson [2001] presented a study which compared 7 isolated substorm injections with 7 storm-time injections using POLAR ENA observations and in situ geosynchronous fluxes. One conclusion of that study

was that, while main phase substorms can be difficult to identify, essentially all storms began with a clear substorm and a clear substorm injection. Further they found that the storm-time injections were essentially identical to isolated substorm injections. They were neither larger (in flux or local time) or more intense (e.g. in spectral hardness). What distinguished storm-times from isolated events was (a) continued injection activity for a period of hours following the initial injection, (b) a spreading of the local time extent of ion injection toward dawn - opposite to the direction of ion drift, and (c) an immediate response in Dst for the storm-time injections compared to no measurable response for the isolated events.

More recently Lui et al. [2001] used Geotail ENA observations of the ring current and SuperDARN radar observations of polar cap convection to study the storm-substorm relationship. They showed that the ring current intensified even at times when there were no substorm injections occurring but that there was simultaneous increase in polar cap convection. Both studies concluded that it was the presence of large-scale, externally-imposed, "convection" electric field superimposed on localized, inductive electric fields which differentiated storm-time particle injections from typical substorm injections – a hypothesis we further investigate in this paper.

A more complete review of recent ENA-based studies of storms and substorms is presented in the introductory paper to this volume [Sharma et al., this volume]. Additionally C:son Brandt et al, [this volume] provide a complementary analysis of the October 2000 storm which uses inversion techniques to calculate the magnetospheric particle distributions and compare the time-dependent magnetospheric energy content with the Dst index.

2. THE OCTOBER 4-6, 2000 STORM

A particularly good storm for investigating the storm-substorm relationship occurred on October 4-6, 2000 (days 278-280). The event began on October 4 (day 278) with a southward turning of the IMF (Plate 1, panel a). B_Z remained moderate at around -10 nT until 04:30 UT on October 5. The moderate driving produced a very gradual build-up of the ring current with Dst decreasing steadily until it reached -142 nT at 19 UT on October 4 (Plate 1, panel b). During that time the solar wind velocity remained below 500 km/s and the density hovered around typical values of 10 particles/cm^3 (data not shown).

For this time period ACE was upstream of the Earth located at X=225, Y=30 R_E while Wind was leading the Earth in its orbit at X=32, Y=-213 R_E. Despite the large perpendicular separations to the Earth, the two spacecraft observed nearly identical solar wind conditions. Plate 1 shows this for B_Z but it was also true for the other parameters which are not shown. Therefore we can be

confident that the solar wind conditions measured were very likely those experienced by the magnetosphere.

In many ways the IMF conditions and the Dst response were characteristic of those which produce so-called Steady Magnetospheric Convection (SMC) events. However, the magnetospheric response was not at all steady as we see from the AE index (panel c) and geosynchronous ion injection data (panel d). Instead, the rather moderate energy input into the magnetosphere allowed substorms to occur at well-separated, roughly two-hour intervals. This gradual development makes it relatively easy to identify individual substorms and to investigate their relationship to the overall dynamics of the storm. (We will present more evidence that this is indeed substorm activity later.)

Throughout the event it is notable how closely the Dst signatures track the solar wind driving. After about 19 UT a gradual weakening of B_Z was accompanied by a weakening of the ring current. A subsequent decrease in B_Z to below 20 nT around 05 UT on October 5 resulted in another decrease in Dst. When the IMF turned northward for a period of about 4 hours, AE became quiet and Dst became less negative (but only recovered to a value around -100 nT). When the IMF turned moderately southward again, Dst reached its minimum of -187 nT around 13 UT. As the IMF B_Z gradually weakened to around zero the recovery of Dst changed slope and AE and injection activity ceased.

We also note the very “direct” response of the ground magnetic perturbations measured by the SYM-H and ASY-H indices which are also plotted in panel b of Plate 1. The SYM and ASY indices are produced from 6 stations and have 1-min time resolution. SYM-H is essentially a higher-resolution version of Dst, is calculated in the same way, and is typically interpreted as the symmetric component of the ring current. It is therefore unremarkable that SYM-H follows the Dst curve and magnitude so faithfully. Here we plot the negative value of ASY-H which is typically interpreted as the asymmetric component of the ring current. -ASY-H is plotted on the same scale as SYM-H and Dst and we see that it also tracks Dst and the solar wind input quite faithfully. While there are times that the magnitude of SYM-H and ASY-H differ by up to a factor of two, it is clear that the two indices are not measuring independent quantities.

We will return to theses points as we examine the main phase of the storm on October 4 in more detail. First we will examine the second substorm injection of the main phase to establish its characteristics and its pedigree as a “substorm” and then consider the effect of the sequence of substorms that occur during the main phase.

3. THE 0930 UT SUBSTORM INJECTION

In order to examine the role of substorms within the storm we first establish that the activity on October 4 has

the characteristic signatures of substorms. Those signatures include auroral brightening and poleward expansion of auroral activity, injection of energetic particles into the inner magnetosphere, stretching and dipolarization of the near-Earth magnetic field, and disruption/diversion of the cross-tail current in the substorm current wedge.

The first injection event of the main phase of this storm took place at 0623 UT approximately 37 min after the southward turning was measured at Wind, which is approximately the time the solar wind would arrive at the magnetopause. The FUV WIC camera on IMAGE showed that, while some auroral activity had started at earlier times, the first auroral brightening and poleward expansion took place at 0611 UT. We will not present data for this substorm/injection event here but rather will concentrate on the second substorm/injection which has nearly identical characteristics but might be considered more representative simply because it is not the first of the sequence.

3.1 Geosynchronous Energetic Particle Injections

Plate 2 shows the geosynchronous measurements and the ground-based indices for the period from 07 to 13 UT on October 4, 2000. The top panel shows energetic electrons (50-315 keV) from spacecraft 1989-046 which was slightly pre-midnight. The next panel shows the protons (75-400 keV) from the same spacecraft. A clear, dispersionless injection occurred at 0938 UT and was simultaneous in both electrons and ions indicating that the satellite, at 2238 LT, was in the heart of the substorm injection region [Reeves et al., 1991; Birn et al., 1997].

Prior to the injection we see a gradual decrease of the energetic electron and ion fluxes from their typical quiet-time values to values about 100 times lower. This is characteristic of a “growth phase dropout” produced by the stretching of the field into a more tail-like configuration [Baker et al., 1978, 1981; Reeves et al., 1993]. However, it is somewhat longer (2 hours) than a typical substorm growth phase. A similar dropout of the geosynchronous energetic particle fluxes begins shortly after the 0938 UT injection producing a “sawtooth” profile.

3.2 Magnetic Field Stretching and Dipolarization

The next panel shows the magnetic field inclination angle from the GOES satellites with 0° representing a completely Earthward-directed field and 90° representing a dipole-like field. Between 0700 and 0938 UT, GOES-10, which was very close to midnight, saw the field stretch from a dipole-like inclination of ≈80° to a very tail-like inclination of ≈10°. Then, between 0934 and 0954 UT the field at GOES-10 recovered to ≈75°. This is the signature of a very clear and strong stretching and dipolarization. GOES-8, which was located 4 hours further east observed qualitatively similar but less intense stretching and

dipolarization. We also note that the nightside field almost immediately began to stretch again in response to continued dayside reconnection so, the nightside magnetic field inclination also exhibits a "sawtooth" profile similar to the energetic particle fluxes. The similarity is expected since the energetic particle "dropout" is produced by the stretching of the field.

3.3 Substorm Current Wedge

The bottom panel of Plate 2 shows the Dst, SYM-H, and -ASY-H indices for this time period. We note again how similar in magnitude and rate of change all three measures of the ground magnetic signatures of the ring current are. Also notable is the change of SYM-H and -ASY-H around the time of substorm onset. This signature is the well-known "mid-latitude H bay" which has long been used as a substorm signature. Turner et al [2000] further investigated this phenomena and also concluded the roughly 25 nT change in the ground magnetic signature is caused by the disruption and diversion of the cross-tail current into the ionosphere in the substorm current wedge.

3.4 Auroral Brightening and Expansion

Plate 3 shows auroral and Energetic Neutral Atom (ENA) images of the substorm collected by the IMAGE spacecraft [Burch et al., 2001]. The Far Ultra-Violet Wideband Imaging Camera (FUV-WIC) auroral imager provides images every two minutes but only representative images are shown here. The orientation is such that the sun is to the right and dusk is to the top of each image. The first image from 0705 UT shows the already expanded auroral oval produced by the earlier substorm. The next two images show the auroral activity dimming and retreating equatorward. The next auroral brightening takes place in the pre-midnight sector at the equatorward edge of the oval at 0930 UT. The auroral brightening expands rapidly poleward within the region of dimmer emissions left over from previous activity. The brightening also expands rapidly in local time until it extends from approximately dusk to well past midnight. By about 0950 a broad oval with regions of localized activity extends around the whole night side. This type if of activity continues until the next substorm in the sequence around 1200 UT.

3.5 ENA Images of the Injection

Plate 3 also gives a global view of the ion injection process seen through ENA images from the Medium Energy Neutral Atom (MENA) and High Energy Neutral Atom (HENA) instruments on IMAGE. Three energy ranges are shown, 5-12, 16-27, and 39-50 keV. In all cases the images show integrated ENA fluxes collected over four minutes and one image is shown each ten minutes beginning at 0930 UT. A "prestorm" image from 0600 UT

is also shown to indicate the quiet-time fluxes and spatial distributions. The color scale is linear and shows the flux of ENA emissions from the line of sight. ENA fluxes are a convolution of the trapped magnetospheric ion distributions and the exospheric neutral density. (C:Son Brandt et al. [this volume] show inversions which determine trapped ion fluxes for this event.)

The MENA images show representative, dipole field lines at L=4 and 8 and the HENA images show dipole field lines at L=4, 8, and 12. Local noon is near the top of the images and is indicated in red for the MENA data and with the label 12 for the HENA data. Slightly different projections are used for the two data sets.

In all three energy ranges the 0930 UT images show effects of activity which began at 0623 UT with the first substorm of the main phase. The 0940 UT images show a clear injection of energetic ions in the pre-midnight region of the inner magnetosphere. To within the 4-minute resolution of these images, this is simultaneous with the injection observed at geosynchronous orbit at 0938 UT and not with the auroral onset which began approximately eight minutes earlier. The ENA emissions intensify between 0940 and 1010 UT which corresponds closely to the increase in ion fluxes measured in situ by the LANL instruments. Subsequently the ENA emissions fade as the particles drift and disperse but the fluxes remain elevated above the 0930 UT levels (See also C:son Brandt et al. [this volume]).

The region of intense ENA emissions also spreads in local time, extending both west, in the direction of ion drift, and east, opposite to the direction of ion drift. The eastward expansion of the ion injection region during storms was first reported by Reeves and Henderson [2001] and is a clear sign of continued Earthward particle transport even after the impulsive injection is over. Some evidence of westward gradient-curvature drift is also visible but during this time scattered sunlight and the viewing geometry make it difficult to unambiguously determine the extent of drift of particles to the dayside magnetosphere. We will examine that issue in more detail in the next section.

The observation of the substorm injection in the ENA emissions makes it clear that the “sawtooth” signatures seen in the geosynchronous observations are true injections and not simply an adiabatic response to the changing local magnetic field. Combined with the auroral images, the GOES magnetic field observations, and the ground magnetic perturbations this provides a fairly complete characterization of a storm-time substorm.

There were eight such substorms during the storm main phase on October 4. Not all spacecraft were well-positioned to make good observations for all eight substorms but, whenever they were, the same signatures we have shown for this substorm were observed in the others and therefore may be typical of storm-time substorms at least under

conditions of moderate driving. We note that similar physical processes probably occur under stronger solar wind driving but the rate of activations makes it difficult or impossible to separate the growth, onset, and recovery phases which characterize isolated substorms.

4. DEVELOPMENT OF THE RING CURRENT

Having examined the injection of ions by substorm processes, let us now look at the overall development of the ring current during the storm main phase on October 4, 2000. Plate 4 shows the geosynchronous energetic ion fluxes, the IMF B_Z, the Dst, SYM-H and -ASY-H indices, and the ENA images from IMAGE and POLAR for the time period from 06 to 24 UT. The ENA images are somewhat different from those in Plate 3. Here we show fluxes for 16-60 keV integrated for 10 minutes and displayed using a logarithmic color scale for the ENA fluxes. One 10-minute image is shown each two hours. Between the 12 and 16 UT images, IMAGE was in the radiation belts and unable to make ENA observations. However, during that time POLAR was well-positioned to make ENA observations (E>37.5 keV) from a similar vantage point. (POLAR made ENA observations at other times which were simultaneous with the IMAGE observations and the two sets of measurements were quite consistent.)

All images are taken from the northern hemisphere and local noon is located near the top of each image. Pixels with known contamination from scattered sunlight have been blacked out but some photon contamination remains in pixels on the dayside at L>8 and those fluxes should be ignored.

At 0600 UT we again see the fairly symmetric, low intensity ENA fluxes prior to the storm which are characteristic of quiet times. Over the next several hours, as Dst decreases, the ENA fluxes intensify. These images provide only a qualitative picture of the energetic ion energy density but C:son Brandt et al, [this volume] show a quantitative analysis which confirms the impression that the energy density in the inner magnetosphere corresponds well with the changes in Dst.

Notice that the geosynchronous ion fluxes (even at their peaks) do not show a long-term build up. However, as we have seen it is the injections at substorm onset that deliver material into the inner magnetosphere. This is understandable if we consider that geosynchronous orbit lies near the transition from dipole to tail field lines. Therefore the fluxes measured there show the particles that are passing through that region as they are transported from the plasmasheet to the inner magnetosphere .

The ENA emissions also allow us to infer the local time distribution of the ring current ions. The images at 0800, 1430 (POLAR), 1600, and 1800 provide particularly good

viewing geometry. At other times, when IMAGE is viewing from the tail toward the dayside, it is not possible to distinguish between ENA fluxes from the dayside equatorial region and ENA fluxes from the high-latitude 'horns' of the nightside field lines without the use of modeling.

However, even given the caveats discussed above it is clear that the ring current development in this storm is highly asymmetric. Up to at least 1800 UT there is little or no evidence of ENA emissions from the dawn-to-noon quadrant of the magnetosphere. Hence there is no truly symmetric component to the ring current in spite of the fact that Dst has been decreasing steadily to less than -120 nT over a period exceeding 10 hours – much longer than ring current ion drift periods. It is likely that the majority of ions injected by substorms on the night side are lost to the magnetopause on the dayside as has been shown through modeling by Liemohn et al, [2001].

The 1600 UT image is particularly striking. ENA fluxes are strongest on the nightside where the injections occur. A "tail" of gradient-curvature drifting ions extends around dusk to the dayside but ends abruptly near Earth-Sun line at noon. Fluxes in the dawn-to-noon sector are extremely low, even as seen on this logarithmic scale. Yet, at 1600 UT, Dst≈-104 nT and the magnitudes of SYM-H and ASY-H were nearly equal at approximately 87 nT. It is clear that all three geomagnetic indices are responding with nearly equal intensity to a highly asymmetric ring current distribution.

5. CONCLUSIONS

In this paper we have examined the geomagnetic storm of October 4-6, 2000. The storm provides an exceptionally good opportunity to examine the role of substorms during the storm because of the relatively moderate solar wind driving and because of the excellent set of satellite observations.

The period on October 4th was characterized a sequence of substorms. We examined one of those substorms in some detail showing that it did, in fact, have the expected signatures of a magnetospheric substorm. The auroral brightening for this substorm was first observed at 0930 UT and the auroral activity subsequently expanded rapidly poleward and in local time. Prior to onset, the nightside magnetic field at geosynchronous orbit was highly stretched with an inclination angle around 10°. At about the same time as the auroral onset a rapid dipolarization of the magnetic field was observed. The diversion of the cross tail current in the substorm current wedge was also observed on the ground as a positive magnetic H bay which also shows up in the 1-minute resolution SYM-H and ASY-H indices.

The injection of energetic particles took place at 0938 UT shortly after the auroral onset and magnetic field

dipolarization. The injection was seen in situ at geosynchronous altitudes and also remotely as a sudden brightening of ENA emissions from the pre-midnight inner magnetosphere.

What then is the role of these substorms in the large-scale spatial and temporal development of the storm-time ring current? It seems clear that one role is the rapid transport of large fluxes of energetic particles from the near-Earth tail into the inner magnetosphere through the effect of inductive electric fields associated with the dipolarization of the magnetic field. This is the traditional view of the role that substorms play in building up the ring current.

However, as we see from Plate 4, Dst had decreased to nearly -50 nT before the 0938 UT injection – after only one substorm injection had occurred – yet isolated substorm injections produce no change in Dst. These results support the conclusions of Reeves and Henderson [2001] who found the same result in a superposed epoch analysis of storm-time and isolated substorm injections.

Clearly other factors contribute to the build-up of the storm-time ring current. The study of Reeves and Henderson suggested that it was the continued injection of ions after onset that distinguished storm-time substorm injections. The ENA observations for October 4 provide further evidence for the role of continued injection. Plate 3 shows that the nightside ENA emissions remain strong and even intensify for almost an hour after onset – even while the magnetic field at GOES is re-stretching. Furthermore the region of nightside injection expands dawnward, opposite to the direction of ion drift, which can only be explained by continued injection.

Reeves and Henderson [2001] suggested that it was the action of the large-scale, quasi-steady "convection" electric field during storm times which was responsible for this continuing injection activity. Lui et al. [2001] reached a similar conclusion based on Geotail ENA and cross-polar cap potential measurements . The observations presented here provide even stronger evidence that it is the combined action of bursty inductive and quasi-steady convective electric fields which produce the storm-time ring current.

Are substorms therefore *essential* to storm development or are they *coincidental*? These observations cannot definitively answer that question but they do provide fodder for speculation. Erickson and Wolf [1980] showed conclusively that it is not possible to adiabatically convect magnetic flux from the distant plasmasheet to the near earth magnetosphere. If the magnetotail starts out with a substantial extent in the anti-sunward direction then substorms seem to be essential to rid the magnetotail of excess plasma and return magnetic flux to the dayside magnetosphere. It seems highly probable that all storms begin with a substorm and we know of no published

evidence showing a storm that did not begin with a substorm.

However, if the neutral line remains not too distant from the Earth and magnetotail does not recover to an extended configuration it may be possible to avoid the Erickson and Wolf "pressure catastrophe". In that case it may be possible for transport of particles and flux to continue without impulsive "unloading" via substorms. This could, then, produce continuation of the storm without subsequent substorms – which has been referred to as steady magnetospheric convection (SMC) events. In fact the storm of October 2000 has the moderate solar wind driving conditions and slow, steady decrease of Dst which are often seen in other events which have been classified as SMCs.

It is sometimes assumed that storms are characterized by the development of a symmetric component to the ring current while substorm injections and SMCs do not trap particles and therefore produce only asymmetric ring current contributions. This is clearly not a useful distinction. For example, it is well-known that isolated substorm injections can produce "drift echoes" in which the injected particles drift through 360° to be observed again at the same spacecraft which is only possible if the particles are "trapped". On the other hand this event produced a dip in Dst (and SYM-H) to below -100 nT over a 10-hour time period without any evidence that the ring current ions were able to drift past midnight to form a symmetric component.

Indeed, while it is possible to separate any azimuthal distribution into symmetric and asymmetric components it may not be terribly informative to do so. This is particularly true if ground magnetic perturbations are used to define the symmetry of the ring current. However, as these observations begin to demonstrate, global observations of the ENA emissions from the ions which actually carry the "ring" current can remove some of the ambiguity which has been an ongoing source of debate. Much as global auroral images have become indispensable to the study of substorms, global ENA images are gradually becoming indispensable to the study of storms. The combination of both along with ground-based and in-situ observations holds great promise for better understanding of the storm-substorm relationship.

Acknowledgments. We would like to thank the many individuals who have provide valuable data and physical insight including the ACE and WIND magnetometer teams, the University of Kyoto, NOAA Space Environment Center and especially John Stienberg, Bern Blake, Terry Onsager, and Howard Singer.

REFERENCES

Baker, D. N., E. W. Hones, Jr., P. R. Higbie, R. D. Belian, and P. Stauning, Global properties of the magnetosphere during a substorm growth phase: A case study, *J. Geophys. Res., 86*, 8941-9856, 1981.

Baker, D. N., P. R. Higbie, E. W. Hones Jr., and R. D. Belian, High-resolution energetic particle measurements at 6.6 Re, 3, Low-energy electron anisotropies and short-term substorm predictions, *J. Geophys. Res., 83*, 4864, 1978.

Barabash, S., P. C:son Brandt, O. Norberg, R. Lundin, E. C. Roelof, C. J. Chase, and B. H. Mauk, Energetic neutral atom imaging by the Astrid microsatellite, *Adv. Space Res., 20*, 1055-1060, 1997.

Birn, J., M. F. Thomsen, J. E. Borovsky, G. D. Reeves, D. J. McComas, and R. D. Belian, Characteristic plasma properties during dispersionless substorm injection at geosynchronous orbit, *J. Geophys. Res., 102*, 2309-2324, 1997.

Burch, J. L., J. L. Burch, S. B. Mende, D. G. Mitchell, T. E. Moore, C. J. Pollock, B. W. Reinisch, B. R. Sandel, S. A. Fuselier, D. L. Gallagher, J. L. Green, J. D. Perez, and P. H. Reiff, Views of Earth's Magnetosphere with the IMAGE Satellite, *Science, 291*, 629, 2001.

C:son Brandt, P., D. G. Mitchell, R. Demajistre, E. C. Roelof, S. Ohtani, J.-M. Janh, C. Polluck, and G. D. Reeves, Storm-substorm relationship during the 4 October, 2000 storm. IMAGE global imaging results, *this volume*.

C:son Brandt, P., R. Demajistre, E. C. Roelof, D. G. Mitchell, and S. Mende, IMAGE/HENA: Global ENA imaging of the plasmasheet and ring current during substorms, *J. Geophys. Res., submitted*, 2002.

C:son Brandt, P., S. Barabash, E. C. Roelof, and C. J. Chase, Energetic neutral atom imaging at low altitude from the Swedish microsatellite Astrid: Observations at low (<=10 keV) energies, *J. Geophys. Res., 106*, 24,663, 2001*a*.

C:son Brandt, P., S. Barabash. E. C. Roelof, and C. J. Chase, Energetic neutral atom imaging at low altitudes from the Swedish microsatellite Astrid: Extraction of the equatorial ion distribution, *J. Geophys. Res., 106*, 25,731, 2001*b*.

Erickson, G. M., and R. A. Wolf, Is steady convection possible in the Earth's magnetotail?, *Geophys. Res. Lett., 7*, 897-900, 1980.

Henderson, M. G., G. D. Reeves, A. M. Jorgensen, H. E. Spence, L. A. Frank, J. B. Sigworth, J. F. Fennell, J. L. Roeder, J. B. Blake, K. Yumoto, K. Shiokawa, and S. Bourdarie, POLAR CEPPAD/IPS energetic neutral atom (ENA) images of a substorm injection, *Adv. Space Res., 25*, 2407-2416, 2000.

Henderson, M. G., G. D. Reeves, K. R. Moore, H. E. Spence, A. M. Jorgensen, J. F. Fennell, J.B. Blake, and E. C. Roelof, Energetic neutral atom imaging with the Polar CEPPAD/IPS instrument: Initial forward modeling results, *Phys. Chem. Earth, 24*, 203, 1999.

Henderson, M. G., G. D. Reeves, H. E. Spence, R. B. Sheldon, A. M. Jorgensen, J. B. Blake, and J. F. Fennell, First energetic neutral atom images from Polar CEPPAD/IPS, *Geophys. Res. Lett., 24*, 1167, 1997.

Jorgensen, A. M., M. G. Henderson, E. C. Roelof, G. D. Reeves, and H. E. Spence, The charge-exchange contribution to the decay of the ring current measured by Energetic Neutral Atoms (ENAs), *J. Geophys. Res., 106*, 1931-1938, 2001.

Jorgensen, A. M., L. Kepko, M. G. Henderson, H. E. Spence, G. D. Reeves, J. B. Sigwarth, and L. A. Frank, The association of energetic neutral atom (ENA) bursts and magnetospheric substorms, *J. Geophys. Res., 105*, 18,753, 2000.

Jorgensen, A. M., H. E. Spence, M. G. Henderson, G. D. Reeves, M. Sugiura, and T. Kamei, Global energetic neutral atom

(ENA) measurements and their association with the Dst index, *Geophys. Res. Lett., 2*4, 3173-3176, 1997.
Liemohn, M. W., J. U. Kozyra, M. F. Thomsen, J. L. Roeder, G. Lu, J. E. Borovsky, and T. E. Cayton, The dominant role of the asymmetric ring current in producing the stormtime Dst*, *J. Geophys. Res., 106*, 10,883-10,904, 2001.
Lui, A. T. Y., R. W. McEntire, and K. B. Baker, A New Insight on the Cause of Magnetic Storms, *Geophys. Res. Lett., 28* , 3413, 2001.
Reeves, G. D., and M. G. Henderson, The storm-substorm relationship: Ion injections in geosynchronous measurements and composite energetic neutral atom images, *J. Geophys. Res., 106*, 5833-5844, 2001.
Reeves, G. D., T. A. Fritz, R. D. Belian, R. W. McEntire, D. J. Williams, E. C. Roelof, M. G. Kivelson, and B. Wilken, Structured plasma sheet thinning observed by Galileo and 1984-129, *J. Geophys. Res., 98*, 21,323, 1993.
Reeves, G. D., R. D. Belian, and T. A. Fritz, Numerical tracing of energetic particle drifts in a model magnetosphere, *J. Geophys. Res., 96*, 13,997, 1991.
Roelof, E. C., Energetic neutral atom image of a storm-time ring current, *Geophys. Res. Lett., 14*, 652, 1987.
Roelof, E. C., D. G. Mitchell, and D. J. Williams, Energetic neutral Atoms (E~50 keV) from the ring current: IMP 7/8 and ISEE 1, *J. Geophys. Res., 90*, 10991, 1985.
Sharma, A. S., and others, Introduction paper to "AGU Monograph on the Storm-Substorm Relationship" (still need the correct title), *this volume.*
Turner, N. E., D. N. Baker, T. I. Pulkkinen, and R. L. McPherron, Evaluation of the tail current contribution to Dst, *J. Geophys. Res., 105*, 5431-5439, 2000.

G. D. Reeves, Los Alamos National Laboratory, NIS-1 MS D-466, Los Alamos, NM 87545. (reeves@lanl.gov)

(Received XXX; revised XXX; accepted XXX)

Paper number XXXX

FIGURE CAPTIONS

Plate 1. Overview of the October 4-6, 2000 geomagnetic storm. (A) the IMF B_Z component (courtesy of the ACE and WIND magnetometer teams). (B) The geomagnetic response measured by the preliminary 1-hour Dst index and by the 1-min. SYM-H and ASY-H components (courtesy of the University of Kyoto). (C) The preliminary AE index as specified by AU and AL (courtesy of the University of Kyoto). (D) The energetic proton flux (75-400 keV) measured by one of the LANL geosynchronous spacecraft.

Plate 2. Characteristics of the 0938 UT substorm injections. Geosynchronous spacecraft 1989-046 was at 22:38 LT when it measured a dispersionless electron (A) and proton (B) injection. Both GOES spacecraft measured a nearly simultaneous dipolarization of the magnetic field (C) and the diversion of the cross-tail current into the ionosphere produced a mid-latitude H bay which also shows up in the SYM-H and ASY-H indices (D)

Plate 3. Auroral and ENA images from the IMAGE spacecraft. The auroral onset measured by the FUV instrument took place at 0930 UT and was followed by a rapid poleward and azimuthal expansion of activity. The substorm injection occurred at 0938 UT and is seen in the 0940 UT ENA images captured by both the MENA and HENA instruments over a wide range of energies.

Plate 4. The development of the ring current relative to the substorm injections from 6-24 UT on October 4. This figure shows energetic proton data, IMF B_Z (from ACE), geomagnetic indices, and ENA images from IMAGE and POLAR. The temporal development and large asymmetry of the ring current are apparent.

Plate 1

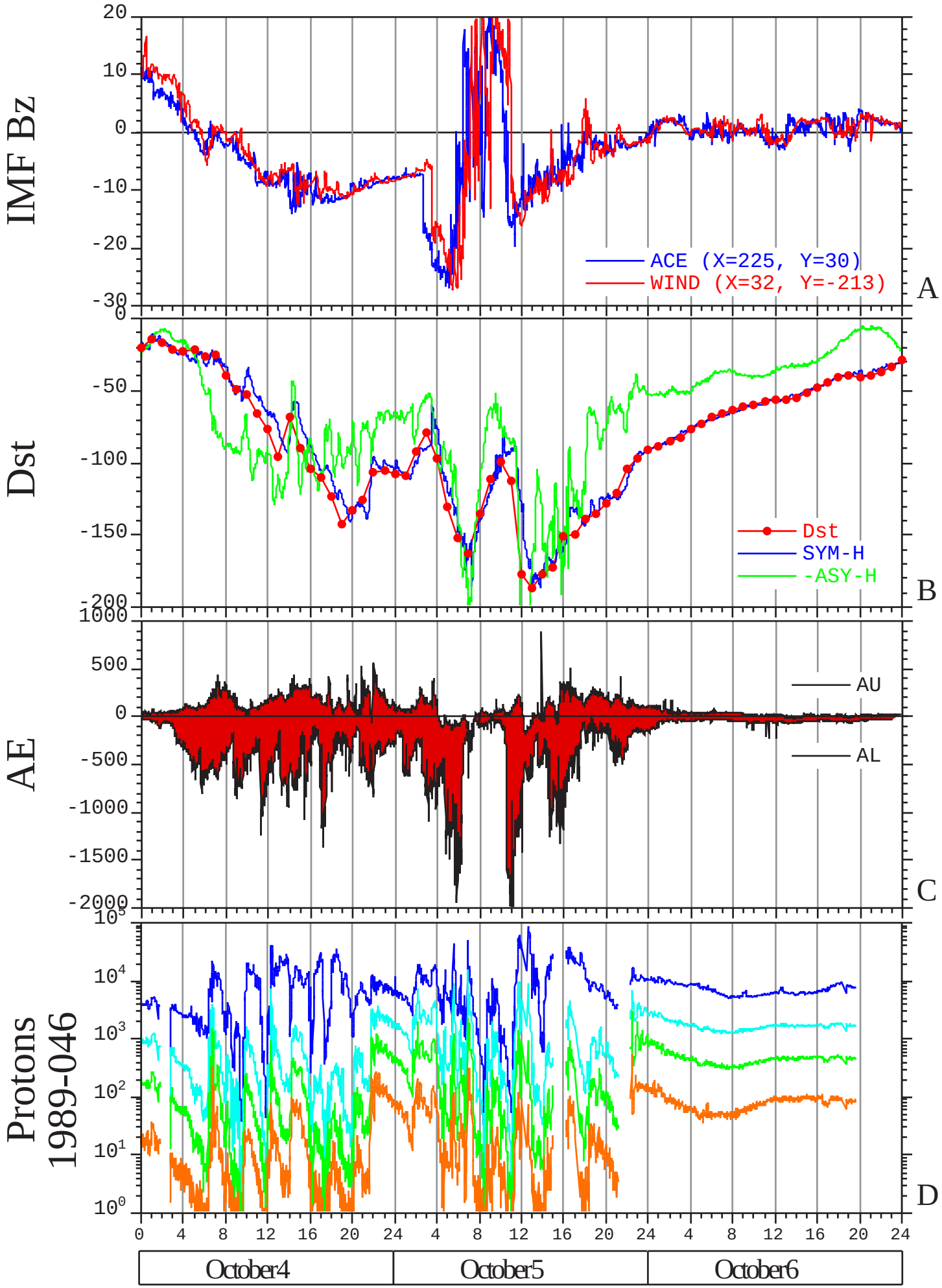
IMF Bz
20
10
0
-10
-20
-30
ACE (X=225, Y=30)
WIND (X=32, Y=-213)
A
Dst
0
-50
-100
-150
-200
Dst
SYM-H
-ASY-H
B
AE
1000
500
0
-500
-1000
-1500
-2000
AU
AL
C
Protons
1989-046
10^5
10^4
10^3
10^2
10^1
10^0
D
0
4
8
12
16
20
24
October4
October5
October6

Plate 2

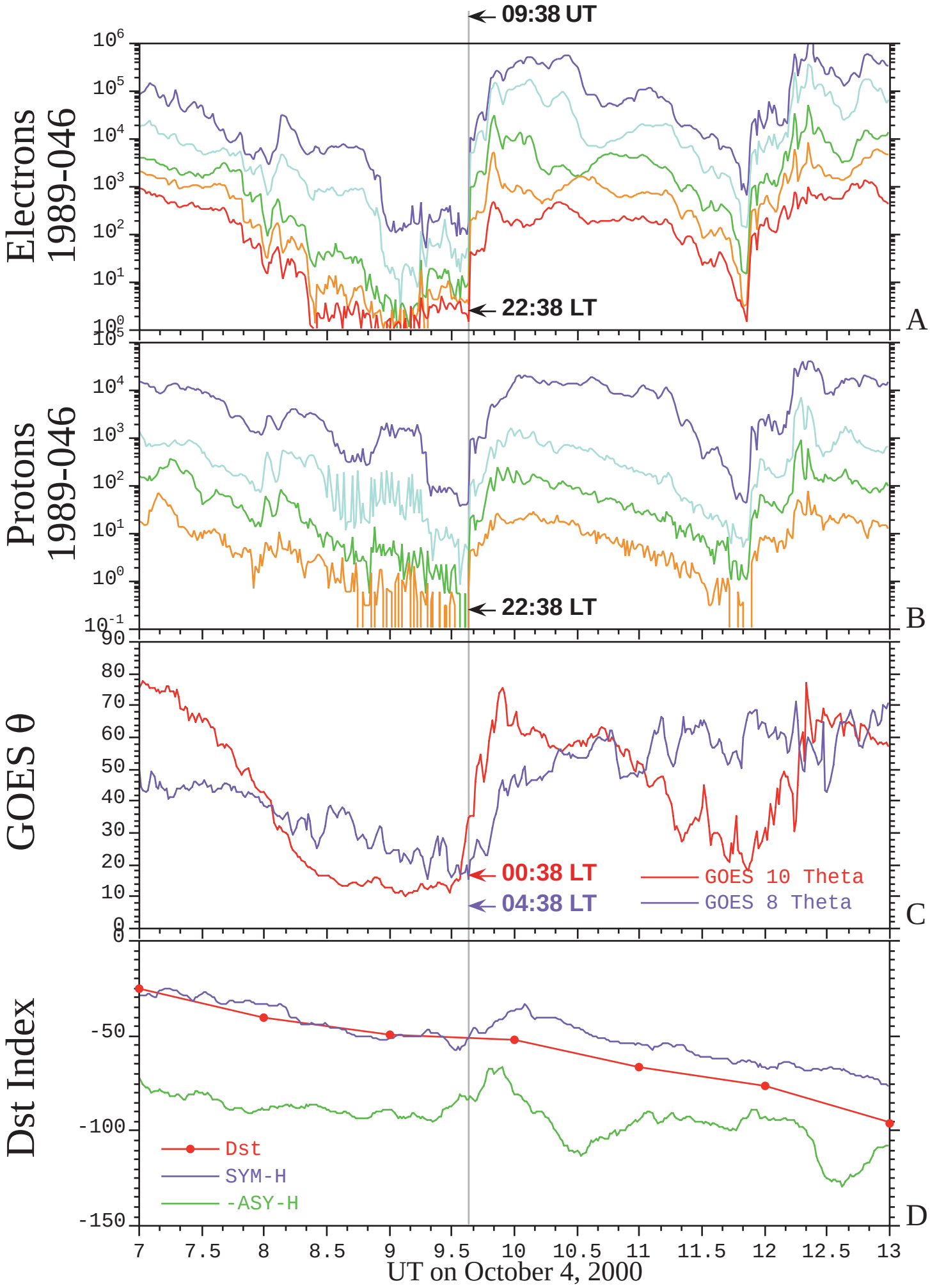
09:38 UT
Electrons 1989-046
22:38 LT
A
Protons 1989-046
22:38 LT
B
GOES θ
00:38 LT
04:38 LT
GOES 10 Theta
GOES 8 Theta
C
Dst Index
Dst
SYM-H
-ASY-H
D
UT on October 4, 2000

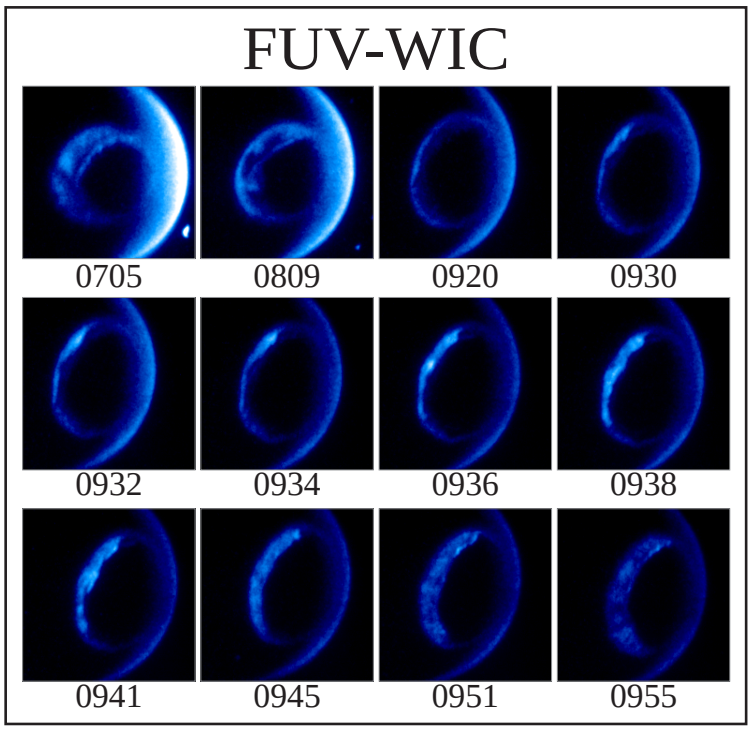
FUV-WIC
0705
0809
0920
0930
0932
0934
0936
0938
0941
0945
0951
0955

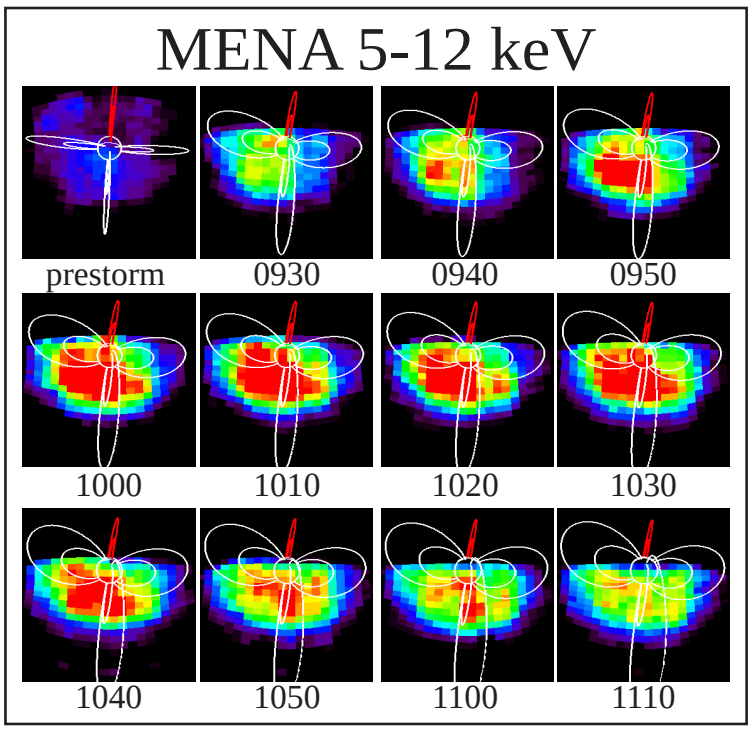
MENA 5-12 keV
prestorm
0930
0940
0950
1000
1010
1020
1030
1040
1050
1100
1110

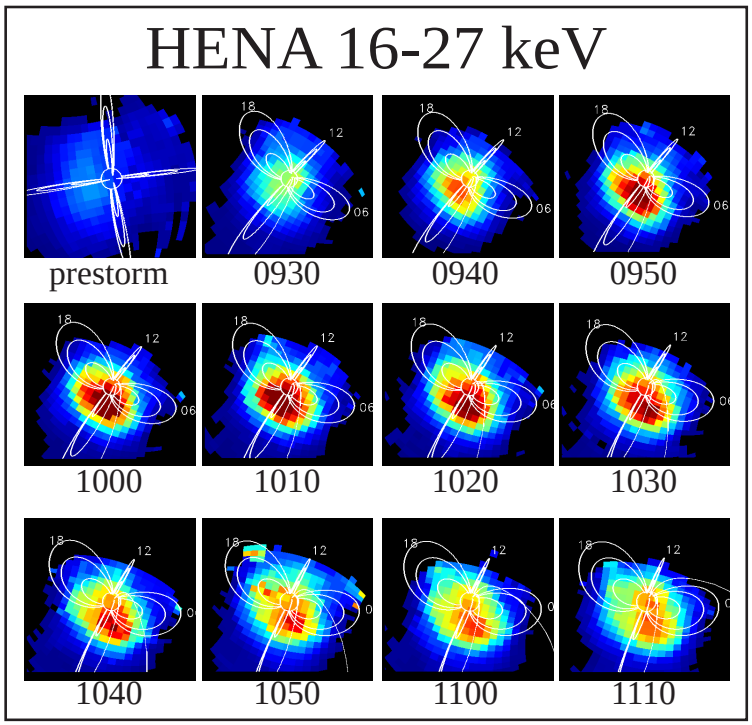
HENA 16-27 keV
prestorm
0930
0940
0950
1000
1010
1020
1030
1040
1050
1100
1110

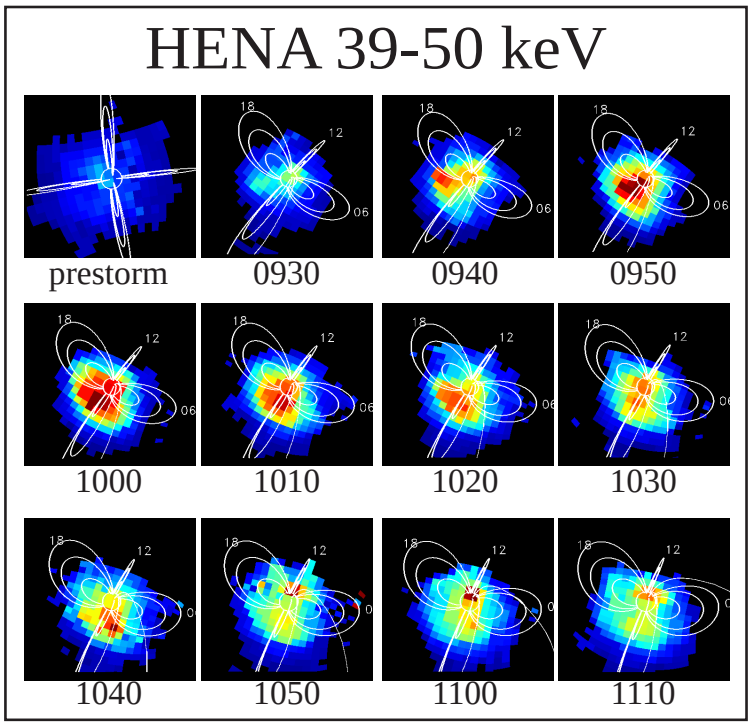
HENA 39-50 keV
prestorm
0930
0940
0950
1000
1010
1020
1030
1040
1050
1100
1110

Plate 3

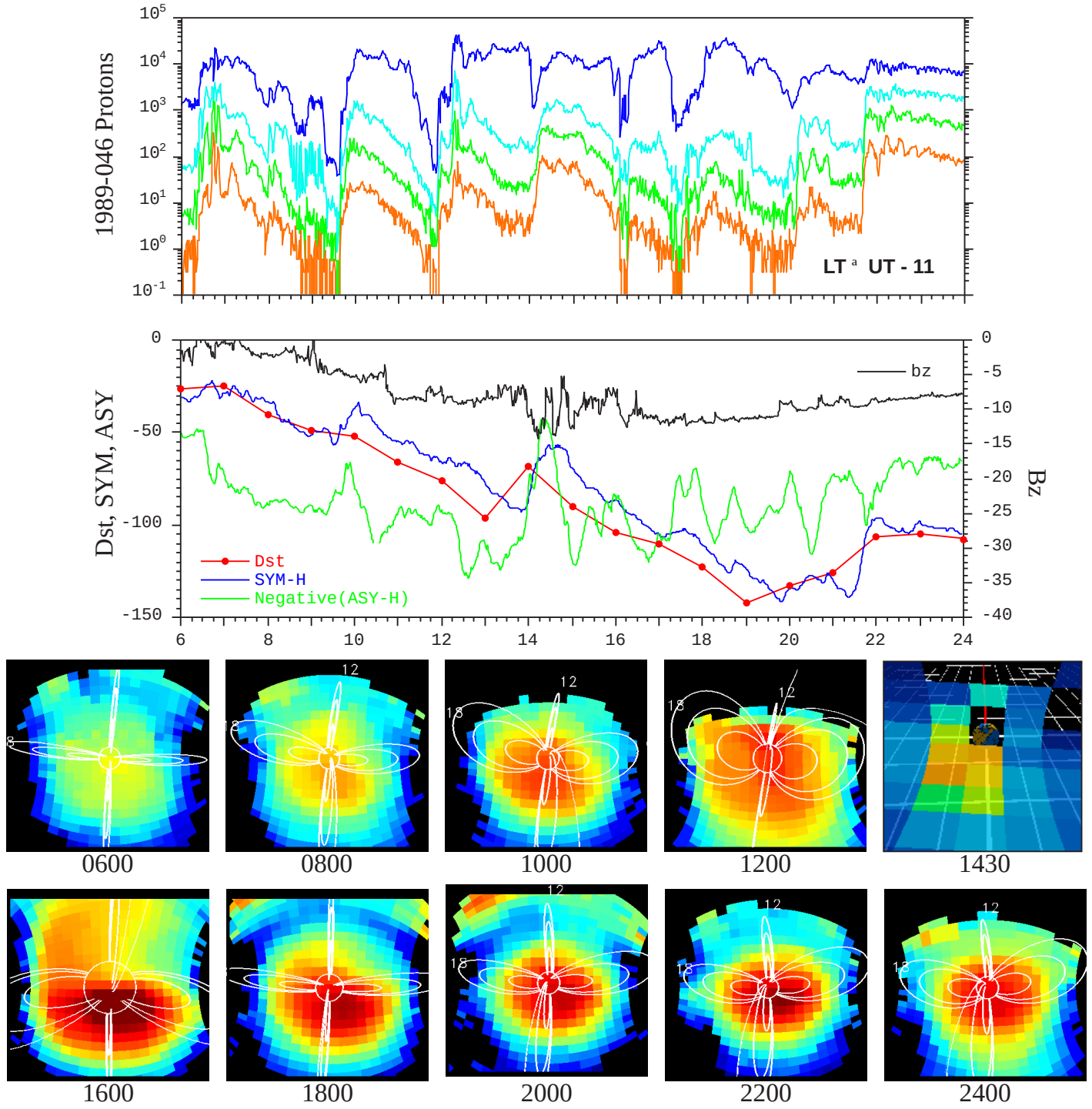
1989-046 Protons
LT a UT - 11
Dst, SYM, ASY
Bz
bz
Dst
SYM-H
Negative(ASY-H)
0600
0800
1000
1200
1430
1600
1800
2000
2200
2400

Plate 4